
Article:
Zheng, M., Zhu, Z.Q. orcid.org/0000-0001-7175-3307, Cai, S. et al. (1 more author) (2019) A novel modular stator hybrid-excited doubly salient synchronous machine with stator slot permanent magnets. IEEE Transactions on Magnetics. ISSN 0018-9464

https://doi.org/10.1109/tmag.2019.2902364

A Novel Modular Stator Hybrid-Excited Doubly Salient Synchronous Machine With Stator Slot Permanent Magnets

M. Zheng[1,2], Z. Q. Zhu[2], S. Cai[2], and S. S. Xue[2]

[1]State Grid Zhejiang Electric Power Research Institute, Hangzhou 310014, China
[2]Department of Electronic and Electrical Engineering, The University of Sheffield, Sheffield S1 3JD, U.K.

This paper presents a novel modular stator hybrid-excited synchronous machine with stator slot permanent magnets (PMs). By regulating the field current, the magnetic field, and consequently the back electromotive force, as well as the average torque can be controlled. The existence of stator slot PMs alleviates the magnetic saturation and improves the flux regulation ratio. The frozen permeability method is employed to investigate the torque contributions by different magnetic sources. Possible stator and rotor pole combinations are illustrated, and the corresponding electromagnetic performances are evaluated with the finite-element method. It is revealed that 12-stator pole machines with 11- and 13-rotor poles exhibit superior average torque and lower torque ripple due to even-order harmonics elimination. Finally, a prototype with modular stator segments is manufactured to validate the analyses and simulations.

Index Terms—**Frozen permeability method (FPM), hybrid-excited machine, modular stator, stator slot permanent magnet (PM).**

I. Introduction

PERMANENT magnet (PM) synchronous machines have attracted extensive attention in the past decades, thanks to the inherent advantages of high torque density, high efficiency, and compact structure [1], [2]. The PMs can be allocated either in stator or in rotor to excite the magnetic field. Recently, the electrical machines with stator PMs are of particular interest due to good heat management and robust rotor structure since all the excitations are stationary [3]–[5]. The concept of locating PMs in the stator slots is first introduced to reduce the magnetic saturation in switched reluctance machine (SRM) [6]. The stator slot PM machine (SSPMM) is further extended to synchronous machine or brushless ac drive, and other stator/rotor pole combinations are discussed in [7], as shown in Fig. 1(a). Since the PM flux is short-circuited in the stator at open circuit, the SSPMM exhibits negligible cogging torque and open-circuit back electromotive force (EMF) without dc excitation. Therefore, the uncontrolled generator fault for conventional PM machines caused by high-induced back EMF at flux-weakening region can be overcome by removing the field excitation [8]–[10].

However, the magnetic field excited by PM is constant and hard to regulate for conventional PM machines. Therefore, hybrid-excited machines, with the combination of PM and dc winding, have been widely investigated [11]–[14]. Since the field coils in rotor demand brushes and slip rings to supply dc excitation, the hybrid-excited machines with field coils in stator are more attractive. In [15], a hybrid-excited SSPMM (HSSPMM) is proposed, as shown in Fig. 1(b). Compared with SSPMM, the HSSPMM exhibits higher power and efficiency at flux-weakening region due to the fact that an extra flexibility is provided to adjust the flux linkage [13]. In addition, high fault-tolerant capability during flux-weakening control at high speed can be achieved by utilizing field excitation current [10].

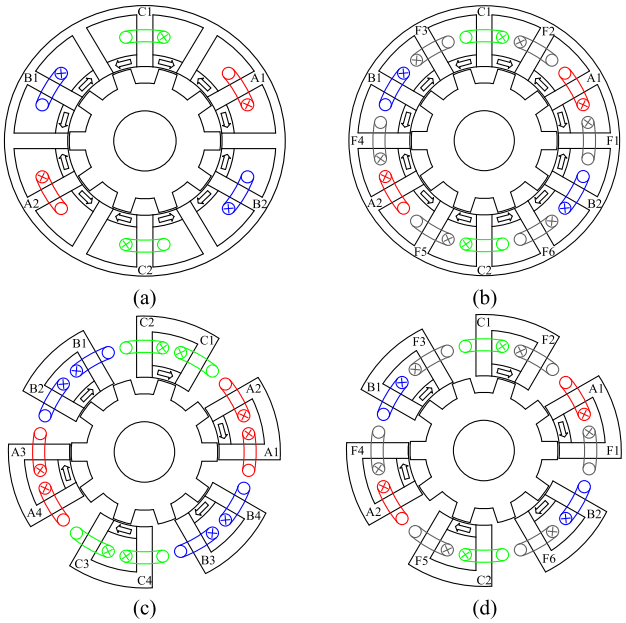

Fig. 1. Cross sections of different SSPMMs. (a) SSPMM [7]. (b) HSSPMM [15]. (c) MS-SSPMM [22]. (d) MS-HSSPMM.

Among the variety of machine topologies, the modular stator counterparts are attractive considering the benefits of manufacturing process, winding packing factor, abandoned punching lamination, convenience for transportation, simplicity of maintenance and fault-tolerant capability [17]–[20]. In [21] and [22], a switched reluctance SSPMM with modular stator-SSPMM (MS-SSPMM) is investigated to facilitate the manufacturing and transportation, as shown in Fig. 1(c). It is revealed that the MS-SSPMM has better over-load capability than MS-SRM due to the existence of PMs.

Manuscript received October 30, 2018; revised February 10, 2019; accepted February 23, 2019. Corresponding author: Z. Q. Zhu (e-mail: z.q.zhu@sheffield.ac.uk).

Color versions of one or more of the figures in this paper are available online at http://ieeexplore.ieee.org.

Digital Object Identifier 10.1109/TMAG.2019.2902364

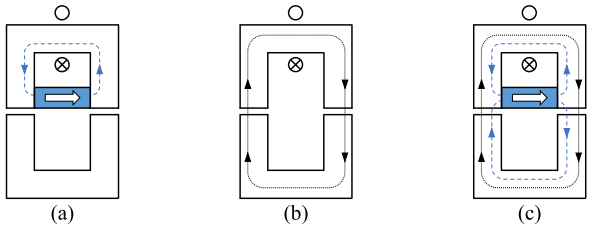

Fig. 2. Schematic of dc and PM flux paths (one modular segment). (a) With PM, $I_{dc} = 0$. (b) Without PM, $I_{dc} > 0$. (c) With PM, $I_{dc} > 0$.

To maintain the benefit of the modular stator technique and achieve controllable flux, a novel MS-HSSPMM is proposed in this paper, as shown in Fig. 1(d). The proposed machine possesses the advantages of SSPMMs, such as negligible PM-excited back EMF and cogging torque, and consequently high fault-tolerant capability. Besides, additional field winding with dc excitation is introduced to regulate the magnetic field according to the output requirement. The PM flux can be pushed to the air gap with field winding excitation, and output capability can be enhanced since the back EMF is produced by both the PM and dc excitations in the proposed machine.

This paper is organized as follows. First, the machine topology and basic operation principle are introduced in Section II. In Section III, the possible stator/rotor pole combinations are discussed based on the EMF vector phasor. Then, in Section IV, the electromagnetic performances with different rotor poles are evaluated with the finite-element method (FEM). Finally, a prototype with modular stator is built, and experiments are carried out to validate the FE predictions.

II. Machine Topology and Operation Principle

A. Machine Topology

As shown in Fig. 1(d), the MS-HSSPMM comprises segmented "U-shape" laminated stator cores and a passive salient-pole rotor without excitations. The PMs are allocated at the slots of the modular stator segments, magnetizing in the same direction. Field coils and armature coils are alternately wound in the stator segment, with non-overlapping end-winding. In addition, the modular stator core construction can eliminate the interaction between different phases, both mechanically and electrically. Since all the magnetic field sources are located in the stator, cooling system can be easily implemented.

B. Operation Principle

The basic operation principle of the proposed machine can be explained by the illustration of single modular segment in Fig. 2. With PM excited only, the flux path is shunted in the stator segment, as shown in Fig. 2(a). With field winding excited only, the flux generated by coil links the rotor and stator via air gap, having opposite direction to the flux produced by PM, as shown in Fig. 2(b). When PM and dc excitations are applied together in Fig. 2(c), the PM flux is pushed to link with rotor due to the magnetic pull by dc excitation. The field excitation current can adjust the magnetic field, and consequently the output capability. Meanwhile, since

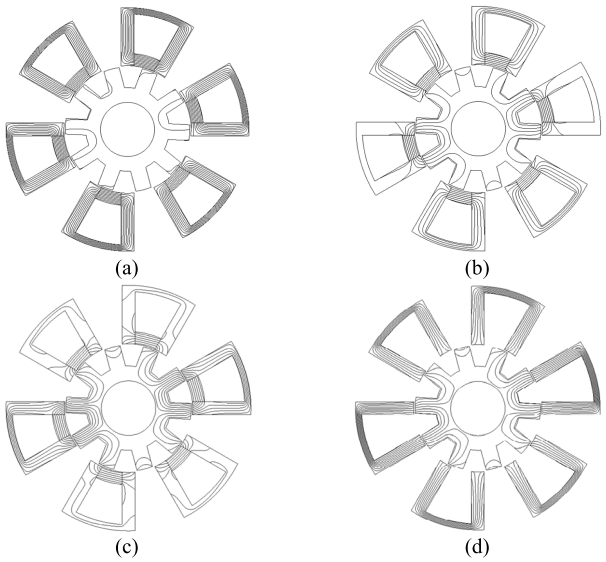

Fig. 3. Open-circuit field distributions in PMs, stator, and rotor cores with different excitations. (a) With PM, $I_{dc} = 0$. (b) With PM, $I_{dc} = 6$ A. (c) With PM, $I_{dc} = 12$ A. (d) Without PM, $I_{dc} = 6$ A.

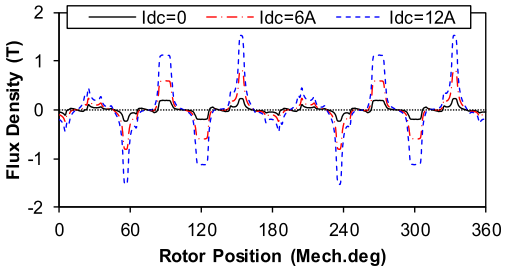

Fig. 4. Open-circuit air-gap flux density waveforms with different dc excitations.

the PM flux is in the opposite direction to DC flux, the PMs at the stator slot can alleviate the magnetic saturation, and further improve the torque density as well as flux regulation capability.

To fully illustrate the flux paths of different sources, the flux line distributions at different excitations are compared in Fig. 3. Without dc excitation, the PM flux is hardly linked with rotor as shown in Fig. 3(a), producing negligible back EMF and cogging torque. As shown in Fig. 3(a)–(c), the flux lines linked with rotor increase with dc excitation current, and the electromagnetic performances can be regulated by dc excitation. Comparing the flux line distributions with/without PM in Fig. 3(b) and (d), the stator magnetic saturation is alleviated by PM excitation.

The open-circuit air-gap flux density and phase back EMF waveforms at different dc excitations are compared in Figs. 4 and 5, respectively. In accordance with the flux line distributions, the air-gap flux density is negligible without dc excitation. With the increase in field current, the flux lines are pushed to link with the salient rotor. As the salient rotor moves, the reluctance as well as flux density varies, producing back EMF in the coils. When corresponding ac current is injected, the machine can output electromagnetic torque.

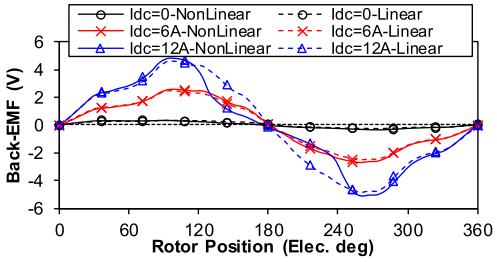

Fig. 5. Open-circuit phase back EMF waveforms with different dc excitations for both the linear and nonlinear stator and rotor materials.

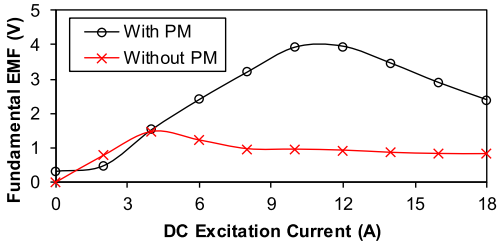

Fig. 6. Open-circuit phase back EMF fundamental versus dc excitation current with/without stator slot PMs.

Therefore, the field current can regulate the air-gap flux density, back EMF, and average torque effectively. Moreover, with the increase in field current, the magnetic saturation becomes severe. Consequently, the back EMF waveforms are deteriorated due to heavy magnetic saturation as the field current increases, and the back EMF waveforms with nonlinear material derive from that with linear material, as shown in Fig. 5.

In order to demonstrate the benefit of employing stator slot PMs, the fundamental phase back EMFs versus dc excitation current with/without PMs are shown in Fig. 6. Without PM excitation, the magnetic circuit becomes saturated at the field current of ~4 A, and the maximum fundamental back EMF is lower than 2 V. With the assistance of PM, the magnetic saturation is alleviated, and the knee point is pulled up. Consequently, both the dc excitation current at knee point and maximum back EMF are improved.

With PM excited only, little flux is linked with rotor, as shown in Fig. 3, and the back EMF is small. As the field current increases, the saturation is reduced and flux density tends to increase reversely. Therefore, with PM and dc excited together, the back EMF regulation ratio is slow at first, then rapid, and finally reduces with the dc excitations.

In addition, the power factors of the proposed machine with/without PMs are shown in Fig. 7. With the increase in field excitation current, the PM and dc jointly excited back EMF are improved in accordance with Fig. 6. Subsequently, the power factor can be improved with $I_d = 0$ control. Furthermore, the introduction of PMs alleviates the magnetic saturation and further enhances the power factor.

C. Average Torque Segregation

As discussed above, multi-sources exist in the hybrid-excited machine, resulting in complex magnetic field

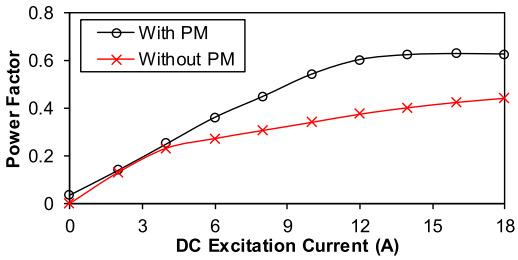

Fig. 7. Power factor versus dc excitation current with/without stator slot PMs at the armature current of $I_d = 0$ and $I_q = 6$ A.

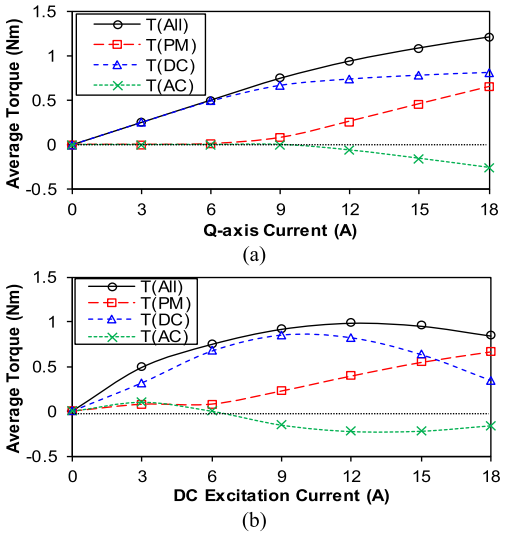

Fig. 8. Average torque separation with FPM. (a) Average torque against the q-axis current with dc excitation current of $I_{\rm dc} = 6$ A. (b) Average torque against dc excitation current with the q-axis current of $I_q = 9$ A.

distribution. To illustrate the main torque contribution, the frozen permeability method (FPM) [23] is employed to segregate the average torque.

The average torque of ac electrical machine is expressed in (1), with $I_d = 0$ control, where p is the number of pole pairs, I_q is the q-axis current, ψ_d(PM), ψ_d(dc), and ψ_d(ac) are the d-axis flux linkage caused by PM, dc, and ac excitations, respectively. According to the contribution of the d-axis flux linkage, the average torque can be segregated by PM synchronous torque T(PM), dc synchronous torque T(dc), and ac armature reaction torque T(ac). It should be noted that T(ac) represents the cross-coupling effect instead of reluctance torque since only I_q is applied

$$\begin{aligned} T_{\rm ave}(I_d = 0) &= \frac{3}{2} p[\psi_d({\rm PM}) + \psi_d({\rm DC}) + \psi_d({\rm AC})]I_q \\ &= T({\rm PM}) + T({\rm DC}) + T({\rm AC}). \end{aligned} \tag{1}$$

Based on the FPM, the d-axis flux linkage can be segregated, and consequently, the average torque of each component is calculated in Fig. 8.

As shown in Fig. 8(a), the average torque increases with the q-axis current, but the increase ratio slows down due to magnetic saturation. When the q-axis current is small, the torque is mainly contributed by dc excitation since the PM

flux is shunted in stator. The ratio of PM torque is increased whereas that of dc torque is reduced with the q-axis current. This can be explained that more PM flux enters the rotor when the stator core is saturated whereas the dc-induced flux linkage is reduced due to large reluctance. Moreover, ac torque is increased reversely, indicating the cross-coupling effect is deteriorated at heavy load.

Meanwhile, as shown in Fig. 8(b), the overall torque increases first and then reduces with the dc excitation current. This can be explained by the over-saturated phenomena [24], since the flux linkage further reduces when the stator and rotor are severely saturated. Similar to the variation shown in Fig. 8(a), the average torque is mainly contributed by dc excitation with small dc excitation current, whereas the PM torque is of higher proportion under magnetic saturation.

III. Combinations of Stator and Rotor Poles

To distribute three phase windings symmetrically, the rotor pole number can be any integer except the multiple of phase number. Thus, the feasible stator pole and rotor pole combinations for a 3-phase 12-stator pole machine can be obtained as 12/8, 12/10, 12/11, 12/13, 12/14, and 12/16 stator/rotor poles. To ensure a short magnetic path in the stator segment, the rotor pole pitch should be close to the stator pole pitch and the rotor pole number approaching the stator tooth number is preferred. Therefore, 12-stator pole machines with 10-, 11-, 13-, and 14-rotor poles are discussed in this paper.

As illustrated in Section II, each stator segment carries one field coil and one armature coil alternatively. Therefore, the number of field coils and armature coils should be $N_s/2$, where N_s is the number of stator teeth. The field coils are allocated of the same polarity, in accordance with the PM magnetization direction. Subsequently, the electrical angle α_e between two adjacent EMF vectors of armature coils can be derived from the mechanical angle α_m, as shown in the following equation. The coil EMF phasors and winding configurations of 12-stator pole machines with 10-, 11-, 13-, and 14-rotor poles are illustrated in Fig. 9

$$\alpha_e = \alpha_m N_r = \frac{2\pi}{N_s/2} \cdot N_r. \tag{2}$$

As shown in Fig. 9, each phase of armature winding consists of two single coils. The flux linkage of coil A1 can be expressed in the Fourier series, as shown in (3). Considering the electrical angular difference between coils A1 and A2, the flux linkage of coil A2 can be expressed in (4):

$$\psi_{\mathrm{A1}} = \sum_{\nu=1,2,3\cdots}^{\infty} \psi_{m\nu} \cos(\nu N_r \Omega_r t + \theta_\nu) \tag{3}$$

$$\psi_{\mathrm{A2}} = \sum_{\nu=1,2,3\cdots}^{\infty} \psi_{m\nu} \cos(\nu N_r \Omega_r t + \theta_\nu + \nu\Delta\theta) \tag{4}$$

where $\Delta\theta$ is the electrical angular difference between coils A1 and A2 and can be expressed as

$$\Delta\theta = \frac{2\pi}{N_s/2} \cdot N_r \cdot \frac{N_s}{4} = N_r\pi. \tag{5}$$

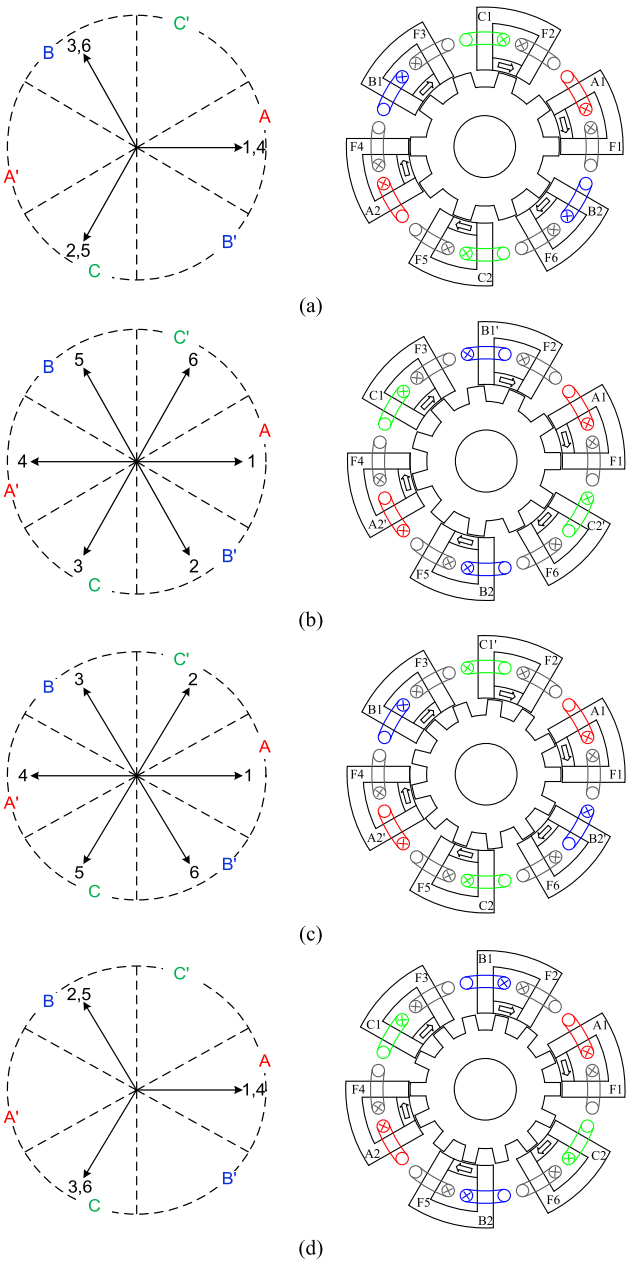

Fig. 9. Coil EMF phasor and machine winding configuration with 12-stator slots and different rotor poles. (a) 10-rotor poles. (b) 11-rotor poles. (c) 13-rotor poles. (d) 14-rotor poles.

Subsequently, the phase flux linkage can be synthesized from single coil flux linkage according to the connection direction, as expressed in the following equation. To maximize the fundamental flux linkage, coils A1 and coil A2 are connected in the same direction for rotor poles of 11 and 13, whereas in the opposite direction for rotor poles of 10 and 14

$$\psi_{\mathrm{A}} = \psi_{\mathrm{A1}} \pm \psi_{\mathrm{A2}}. \tag{6}$$

According to (3)–(6), it can be concluded that the even-order harmonics in the phase flux linkage are canceled, when coils A1 and A2 are connected reversely. The EMF phasors of coils A1 and A2 with the rotor pole of N_r = 11 and N_r = 13

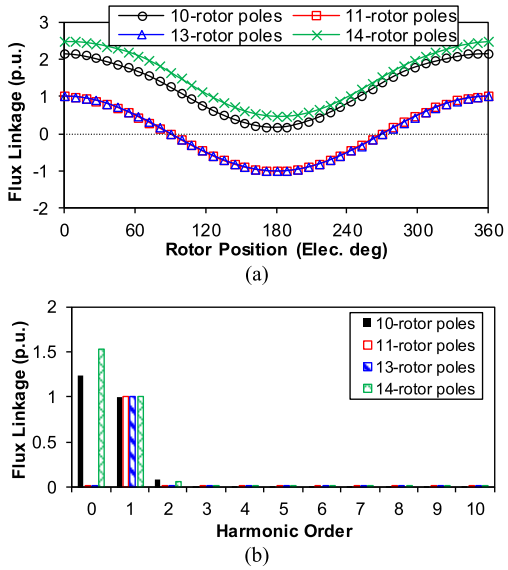

Fig. 10. Normalized open-circuit phase flux linkage for the 12-stator poles MS-HSSPMMs with different rotor poles under the excitation of PM and field winding. (a) Waveforms. (b) Spectra.

are in the opposite direction as shown in Fig. 9, and therefore, the even-order harmonics are absent in phase flux linkages.

To validate the theoretical analyses, FE calculation is conducted for the MS-HSSPMMs with different rotor poles. The normalized open-circuit phase flux-linkage waveforms and spectra are illustrated in Fig. 10. The phase flux linkages of MS-HSSPMMs with 10- and 14-rotor poles are unipolar. On the contrary, the 11- and 13-rotor pole machines have bipolar phase flux linkage and even-order harmonics are canceled.

IV. Performance Comparison

In this section, the MS-HSSPMMs with different rotor poles are globally optimized for maximum average torque, and the electromagnetic performances are further compared.

To gain a fair comparison, the MS-HSSPMMs with 10-/11-/13-/14-rotor poles are optimized with the constraint of fixed stator outer diameter of 90 mm, stack length of 25mm, air-gap length of 0.5 mm, slot packing factor of 0.59, and total copper loss of 60 W. To simplify the analysis, the field coils and armature coils occupy half of the stator slots. Subsequently, the copper loss of field winding and armature winding can be expressed as follows:

$$p_{\mathrm{Cu}} = \frac{\rho_{\mathrm{Cu}} \cdot N_s \cdot L_s \cdot N_{\mathrm{fc}}^2 \cdot I_{\mathrm{dc}}^2}{S_c \cdot k_p} + \frac{\rho_{\mathrm{Cu}} \cdot N_s \cdot L_s \cdot N_{\mathrm{ac}}^2 \cdot I_{\mathrm{ac}}^2}{2S_c \cdot k_p} \quad (7)$$

where ρ_{Cu} is the copper electrical resistivity, L_s is the stack length, S_c is the single slot area, k_p is the packing factor, N_{fc} is the number of turns per field coil, N_{ac} is the number of turns per armature coil, and I_{dc} and I_{ac} are the amplitudes of dc and ac excitations, respectively.

The optimization is carried out based on the genetic algorithm embedded in the commercial software Ansys Maxwell. After global optimization, the main parameters are listed in Table I.

TABLE I
Main Parameters of Optimized MS-HSSPMM With Different Rotor Poles

Parameter	Unit	N_r=10	N_r=11	N_r=13	N_r=14
Stator Outer Diameter	mm	90			
Stack Length	mm	25			
Air-gap Length	mm	0.5			
Total Copper Loss	W	60			
Packing Factor	-	0.59			
Turns per Armature Coil	-	92			
Turns per Field Coil	-	92			
Split Ratio	-	0.51	0.54	0.54	0.53
Stator Yoke Thickness	mm	2.3	2.6	2.5	2.4
Stator Pole Arc	°	11.5	10.2	9.0	9.0
Rotor Pole Arc	°	14.5	13.3	10.2	10.2
Rotor Tooth Height	mm	4.5	4.5	4.5	4.5
PM Height	mm	4.5	3.7	3.9	3.9
PM Volume	mm^3	5991	5250	5948	5932
PM Remanence	T	1.23			
PM Coercivity	kA/m	932			

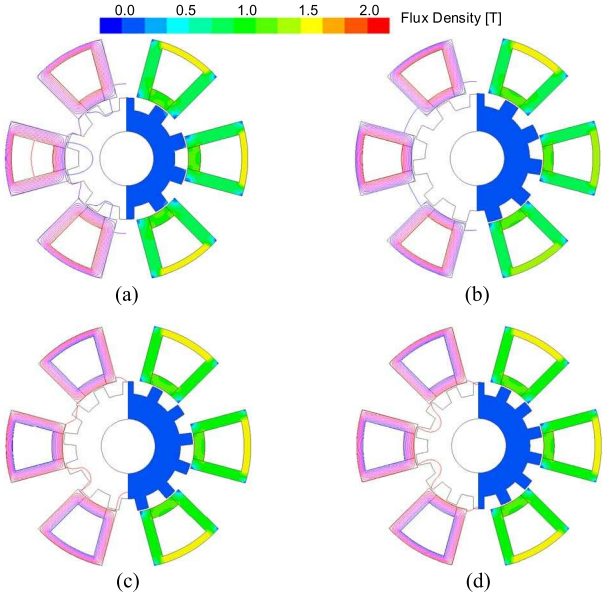

Fig. 11. Open-circuit field distributions of MS-HSSPMMs with different rotor poles. (a) 10-rotor poles. (b) 11-rotor poles. (c) 13-rotor poles. (d) 14-rotor poles.

A. Open-Circuit Field Distribution

The open-circuit field distributions of the MS-HSSPMMs with different rotor poles are shown in Fig. 11. The PM flux mainly shunts in the stator, regardless of rotor poles. The flux density in stator body is around 1.0–1.5 T at open-circuit, and the flux in rotor is negligible. Therefore, the open-circuit back EMFs are very small, making them attractive in high-speed safety-critical application.

B. Back EMF

Without dc excitation, the PM flux hardly links with rotor. When dc excitation is applied, the flux is pushed to link with the salient rotor. With the dc excitation of copper loss $p_{\mathrm{dc}} = 30$ W, the open-circuit back EMFs for different rotor

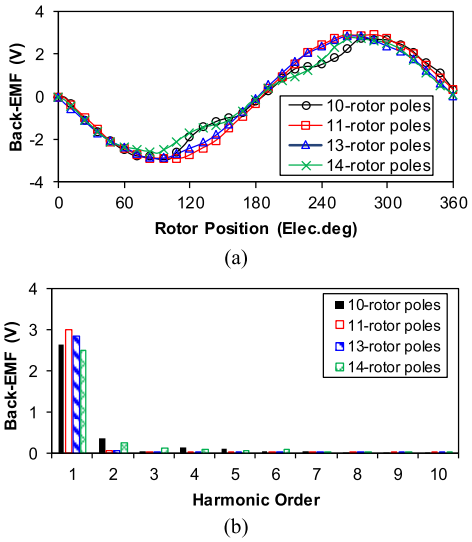

Fig. 12. Open-circuit phase back EMF for the 12-stator pole MS-HSSPMMs with different rotor poles under the field winding copper loss of $p_{dc} = 30$ W at the rotor speed of 400 r/min. (a) Waveforms. (b) Spectra.

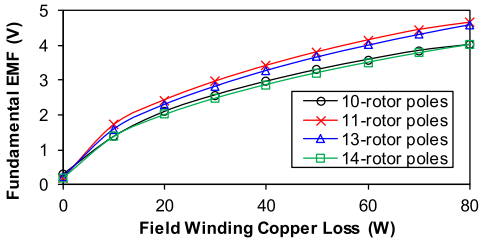

Fig. 13. Open-circuit phase back EMF fundamentals against field winding copper loss for MS-HSSPMMs with different rotor poles at the rotor speed of 400 r/min.

poles are compared in Fig. 12. The fundamental back EMF for 11- and 13-rotor pole machines is higher than that of 10- and 14-rotor pole machines. In addition, the harmonics are more abundant in 10- and 14-rotor pole machines. As illustrated in Section III, even-order harmonics exist in the phase flux linkage as well as back EMF of 10- and 14-rotor pole machines. The even-order harmonics deteriorate the back EMF waveform and further result in an additional pulsating torque component.

The open-circuit phase back EMF fundamentals against field winding copper loss at the rotor speed of 400 r/min are illustrated in Fig. 13. Without dc excitation, the back EMF fundamentals are negligible regardless of rotor poles. The back EMF can be regulated by the field current and increases with the field winding copper loss. Moreover, it can be observed that the fundamental back EMFs of 11- and 13-rotor pole machines are higher than those of 10- and 14-rotor pole machines during the whole field winding copper loss.

C. Inductance

The d-axis and q-axis inductances against corresponding current for different rotor pole machines are compared in Fig. 14. It is obvious that both the d-axis and q-axis inductances reduce with corresponding current due to magnetic saturation. In addition, the d-axis and q-axis inductances are similar, resulting in negligible reluctance torque.

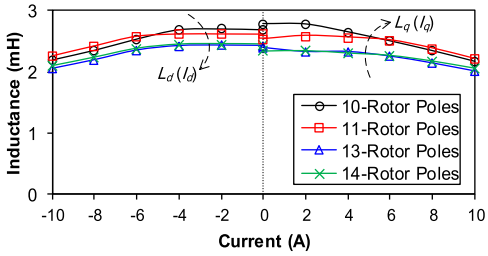

Fig. 14. d-axis and q-axis inductances versus d-axis and q-axis currents for different rotor poles.

TABLE II
SELF-INDUCTANCE AND MUTUAL INDUCTANCE BETWEEN PHASES

	$N_r = 10$	$N_r = 11$	$N_r = 13$	$N_r = 14$
Self-Inductance	2.18 mH	2.06 mH	1.95 mH	2.12 mH
Mutual-Inductance	0.04 mH	0.02 mH	0.02 mH	0.02 mH

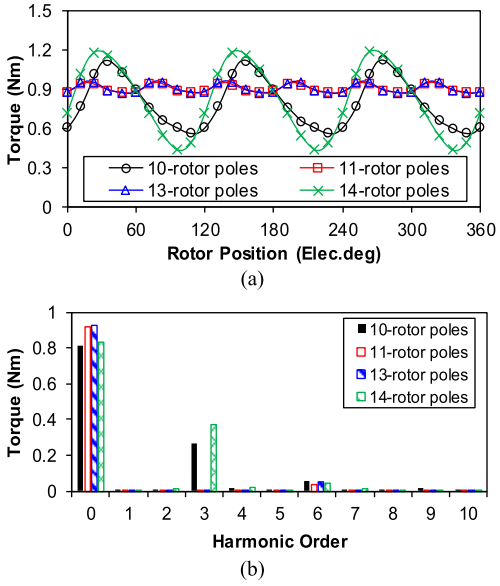

Fig. 15. Electromagnetic torques for the 12-stator pole MS-HSSPMMs with different rotor poles under the field and armature winding copper losses of $p_{dc} = p_{ac} = 30$ W. (a) Waveforms. (b) Spectra.

Moreover, the self-inductance and mutual inductance between phases are listed in Table II. Since the flux paths of different phases are cutoff by the modular stator structure, the mutual inductances are very small, and the cross-coupling effect between phases is avoided.

D. On-Load Torque

The electromagnetic torque at the load of $p_{ac} = p_{dc} = 30$ W and $I_d = 0$ control with different rotor poles is predicted in Fig. 15. The average torques of 11- and 13-rotor pole machines are higher than those of 10- and 14-rotor pole machines, in accordance with back EMF analyses. In addition, the torque ripples of 10- and 14-rotor pole machines are significantly larger than those of 11- and 13-rotor pole machines. The dominant pulsating torques in 10- and 14-rotor pole machines are the third-order harmonic, whereas the lowest pulsating torques are the sixth-order for the 11- and 13-rotor pole machines.

To illustrate the torque pulsating component, the instantaneous electromagnetic torque with ideal sine-wave current

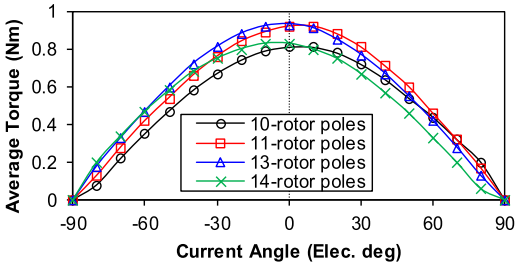

Fig. 16. Average torques versus armature winding current angle for the 12-stator pole MS-HSSPMMs with different rotor poles under the field and armature winding copper losses of $p_{\rm dc} = p_{\rm ac} = 30$ W.

drive is derived in the following equation when $I_d = 0$ control is utilized and on-load magnetic saturation is neglected:

$$T_e = \frac{e_a i_a + e_b i_b + e_c i_c}{\omega_r} + T_c = \frac{3 I_m E_1}{2\omega_r} + \frac{3 I_m E_{3k-1} \cos 3k\omega_e t}{2\omega_r} + \frac{3 I_m E_{3k+1} \cos 3k\omega_e t}{2\omega_r} + T_c. \quad (8)$$

Since there exists significant second-order harmonic in the back EMF for 10- and 14-rotor poles, as shown in Fig. 12(b), the third pulsating torque is produced according to (8). The third pulsating torque is of low order and high amplitude, which has detrimental effect on the output torque performance. Therefore, the 11- and 13-rotor pole machines are superior considering the average torque and torque ripple in comparison with 10- and 14-rotor pole machines.

The average torques versus current angle with the excitation of $p_{\rm ac} = p_{\rm dc} = 30$ W are shown in Fig. 16. The optimal current angle is almost 0, indicating the reluctance torque is negligible for the proposed MS-HSSPMMs.

To further investigate the optimal copper loss distribution within the fixed copper loss, the average torques against field winding copper loss ratio with $p_{\rm dc} + p_{\rm ac} = 60$ W are shown in Fig. 17. The optimal field winding copper loss is about 0.4–0.5 regardless of rotor poles.

In addition, the average torques versus armature winding copper loss with the field copper loss of $p_{\rm dc} = 30$ W are shown in Fig. 18. When the armature current is small, the 11- and 13-rotor poles machines exhibit similar torque density. However, the 13-rotor pole machine has better overload capability, and the average torque is higher under heavy load.

Moreover, the average torques versus field winding copper loss with the armature copper loss of $p_{\rm ac} = 30$ W is shown in Fig. 19. Without dc excitation, the average torques of four machines are similar. The field current can regulate the back EMF as well as average torque. The 13-rotor pole machine exhibits better flux regulation capability, and the average torque is the highest with large field excitation current.

V. Experimental Validation

To validate the theoretical analyses and FE-predicted results, a prototype of 12/11 stator/rotor poles is fabricated and tested in this section.

A. Prototype

The photographs of the prototype are shown in Fig. 20(a)–(d), and the main parameters are kept the same as shown in Table I. To accurately locate the modular stator segment, a fin is designed on the outer surface of the modular stator yoke, as shown in Fig. 20(a). Correspondingly, the stator frame has notches in its inner surface, which matches the fins and contour of stator segment, as shown in Fig. 20(b). Thanks to the modular stator technique, the abandoned punching laminated materials can be saved compared with entire stator core. Moreover, each stator segment is pre-wound with tooth coil field and armature windings alternatively, which simplified the winding process. To verify the theoretical analysis as well as the FE simulation, the packing factor is chosen as 0.3 for the academic laboratory hand-wound coils, although higher packing factor can be achieved for industrial mass production with a modular technique [25], [26]. Special attention should be paid for the winding to avoid exposed coil side insulation damage. The PMs have been designed as the same size and shape with the stator slot opening, and are glued between stator teeth. In addition, the PMs also operate as the slot wedge, preventing the coils running into the air gap. Finally, the assembled stator, including stator slot PMs, field windings, and armature windings, is illustrated in Fig. 20(c).

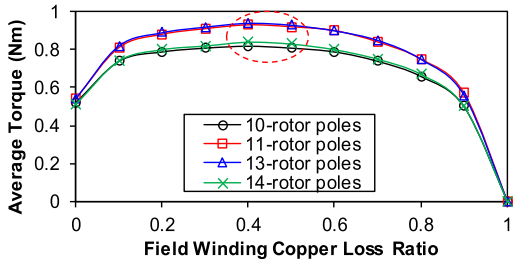

Fig. 17. Average torques versus field winding copper loss ratio for the 12-stator pole MS-HSSPMMs with different rotor poles under the fixed copper losses summary of $p_{\rm dc} + p_{\rm ac} = 60$ W.

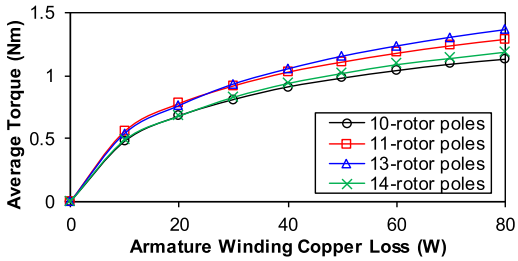

Fig. 18. Average torques versus armature winding copper loss for the 12-stator pole MS-HSSPMMs with different rotor poles under the field copper losses of $p_{\rm dc} = 30$ W.

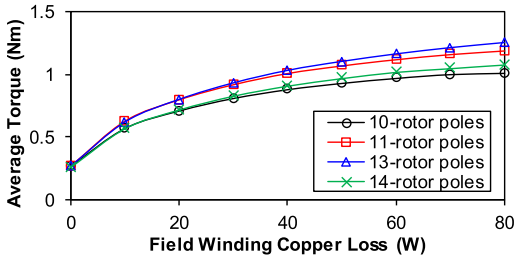

Fig. 19. Average torques versus field winding copper loss for the 12-stator poles MS-HSSPMMs with different rotor poles under the armature copper losses of $p_{\rm ac} = 30$ W.

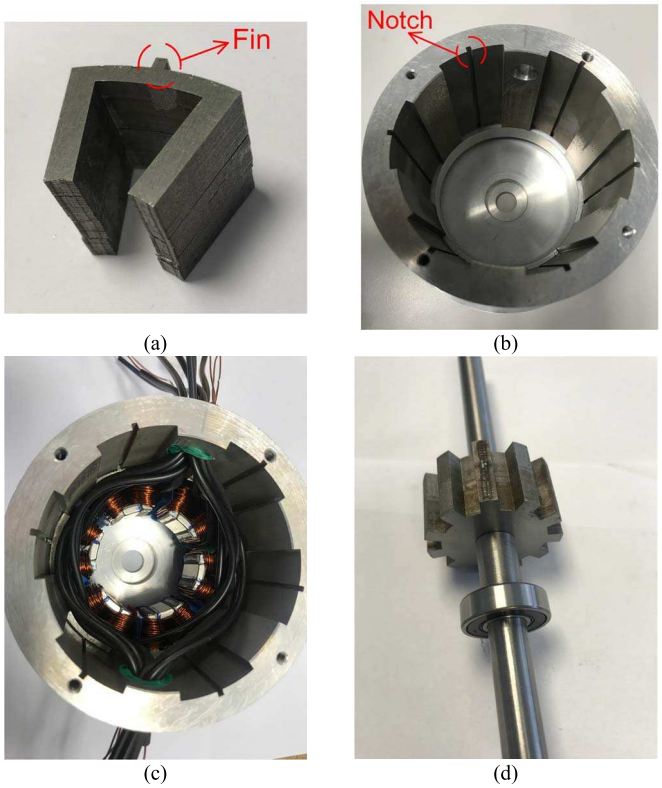

Fig. 20. Photographs of 12-/11-stator slots/rotor poles MS-HSSPMM prototype. (a) Stator core segment. (b) Stator frame. (c) Assembled stator. (d) Rotor.

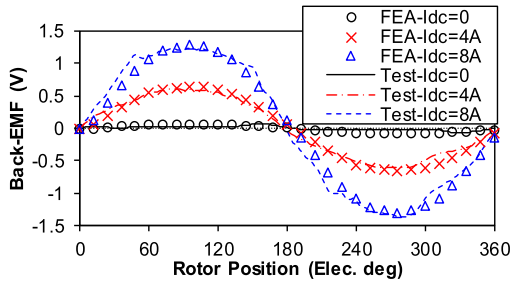

Fig. 21. Measured and FE-predicted open-circuit phase back EMF waveforms with different dc excitation currents at the rotor speed of 400 r/min.

B. Back EMF

At the rotor speed of 400 r/min, the measured and FE-predicted open-circuit back EMF waveforms are shown in Fig. 21. The phase back EMF fundamental versus field excitation current is further illustrated in Fig. 22. Without field current excitation, the back EMF is negligible for both FE and test results. In addition, the back EMF is increased with the dc excitation current, in accordance with the theoretical analyses. Overall, the test results agree well with the FE predictions. The error between finite element analysis (FEA) test results can be explained by the manufacturing tolerance and the 3-D end effect.

C. Static Torque

To validate the output torque capability, the static torque is measured based on the method proposed in [27]. With the armature winding excitation of $I_a = -2I_b = -2I_c$, the static torque is measured at different rotor positions, as shown in Fig. 23.

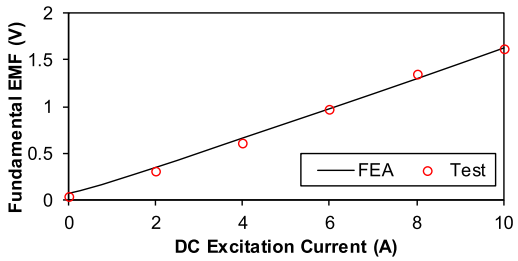

Fig. 22. Measured and FE-predicted open-circuit phase back EMF fundamentals against dc excitations at the rotor speed of 400 r/min.

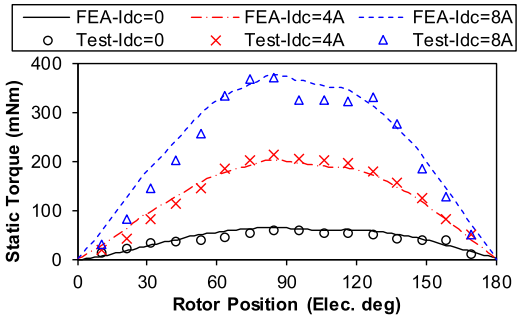

Fig. 23. Measured and FE-predicted static torque waveforms with various field winding excitations ($I_{\rm dc}$) at the fixed armature winding current of $I_A = -2I_B = -2I_C = 8$ A.

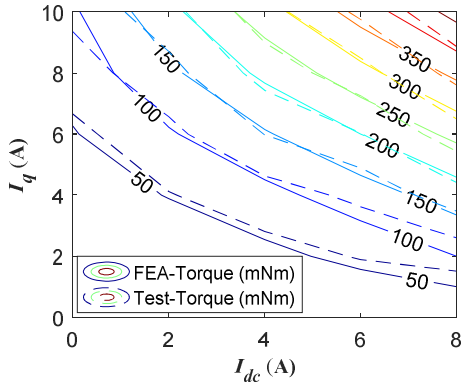

Fig. 24. Measured and FE-predicted torques with various dc excitation currents and q-axis currents.

The static torque can be regulated by the field current and the test results agree well with the FE-predicted results. The difference between predicted and measured results can be explained by the manufacturing and assembling tolerance. Especially for electrical machines with modular stator structure, additional air gaps exist between stator segments [28], [29].

Finally, the rotor is fixed to align the rotor q-axis with stator armature winding phase-A axis, and the phase currents of $I_A = -2I_B = -2I_C$ are applied to the armature winding. The d-axis and q-axis currents can be derived in the following equation in which θ is the electrical angle between the phase-A axis and the d-axis, viz., $-\pi/2$:

$$\begin{bmatrix} i_d \\ i_q \\ i_0 \end{bmatrix} = \frac{2}{3}\begin{bmatrix} \cos\theta & \cos\left(\theta - \frac{2}{3}\pi\right) & \cos\left(\theta + \frac{2}{3}\pi\right) \\ -\sin\theta & -\sin\left(\theta - \frac{2}{3}\pi\right) & -\sin\left(\theta + \frac{2}{3}\pi\right) \\ \frac{1}{2} & \frac{1}{2} & \frac{1}{2} \end{bmatrix} \times \begin{bmatrix} i_a \\ i_b \\ i_c \end{bmatrix} = \begin{bmatrix} 0 \\ I_A \\ 0 \end{bmatrix}. \quad (9)$$

Therefore, the torques with different dc excitation currents and q-axis currents can be measured in comparison with FE prediction, as shown in Fig. 24. The torque can be controlled by dc excitation and the q-axis current. Again, the test results agree well with FE predictions.

VI. Conclusion

This paper proposes a novel modular stator hybrid-excited stator slot PM synchronous machine. The proposed topology benefits from the modular stator technique, which facilitates manufacturing, assembling, and transportation. In addition, the modular stator structure cuts off the mechanical, electrical, and magnetic connection between different phases, and subsequently, high fault-tolerant capability is achieved.

The PMs are located in the stator slots to alleviate the magnetic saturation. Since the PM flux is short-circuited in the stator segment, the cogging torque and back EMF are negligible. In addition, field windings have been attached to regulate the magnetic field and output capability. It is revealed that the average torque is mainly contributed by dc excitation at light load, whereas the ratio of PM synchronous torque is larger with heavy load.

Moreover, different combinations of stator and rotor poles are discussed, and the condition to eliminate even-order harmonic is concluded. The electromagnetic performances of the MS-HSSPMMs with different rotor poles are evaluated with FE simulations. It is shown that the 11- and 13-rotor pole machines exhibit superior average torque and smoother torque ripple.

Finally, a 12-/11-stator/rotor pole prototype with modular stator is fabricated and tested. The test results agree well with the FE predictions, verifying the theoretical analyses and simulations.

References

[1] K. T. Chau, C. C. Chan, and C. Liu, "Overview of permanent-magnet brushless drives for electric and hybrid electric vehicles," *IEEE Trans. Ind. Electron.*, vol. 55, no. 6, pp. 2246–2257, Jun. 2008.

[2] N. Bianchi, E. Fornasiero, and W. Soong, "Selection of PM flux linkage for maximum low-speed torque rating in a PM-assisted synchronous reluctance machine," *IEEE Trans. Ind. Appl.*, vol. 51, no. 5, pp. 3600–3608, Sep./Oct. 2015.

[3] R. P. Deodhar, S. Andersson, I. Boldea, and T. J. E. Miller, "The flux-reversal machine: A new brushless doubly-salient permanent-magnet machine," *IEEE Trans. Ind. Appl.*, vol. 33, no. 4, pp. 925–934, Jul./Aug. 1997.

[4] R. Cao, C. Mi, and M. Cheng, "Quantitative comparison of flux-switching permanent-magnet motors with interior permanent magnet motor for EV, HEV, and PHEV applications," *IEEE Trans. Magn.*, vol. 48, no. 8, pp. 2374–2384, Aug. 2012.

[5] Z. Q. Zhu and J. T. Chen, "Advanced flux-switching permanent magnet brushless machines," *IEEE Trans. Magn.*, vol. 46, no. 6, pp. 1447–1453, Jun. 2010.

[6] K. Nakamura, K. Murota, and O. Ichinokura, "Characteristics of a novel switched reluctance motor having permanent magnets between the stator pole-tips," in *Proc. Eur. Conf. Power Electron. Appl.*, Aalborg, Denmark, Sep. 2007, pp. 1–5.

[7] I. A. A. Afinowi, Z. Q. Zhu, Y. Guan, J. C. Mipo, and P. Farah, "Electromagnetic performance of stator slot permanent magnet machines with/without stator tooth-tips and having single/double layer windings," *IEEE Trans. Magn.*, vol. 52, no. 6, Jun. 2016, Art. no. 8103410.

[8] T. M. Jahns and V. Caliskan, "Uncontrolled generator operation of interior PM synchronous machines following high-speed inverter shutdown," *IEEE Trans. Ind. Appl.*, vol. 35, no. 6, pp. 1347–1357, Nov. 1999.

[9] G. Pellegrino, A. Vagati, and P. Guglielmi, "Design tradeoffs between constant power speed range, uncontrolled generator operation, and rated current of IPM motor drives," *IEEE Trans. Ind. Appl.*, vol. 47, no. 5, pp. 1995–2003, Sep./Oct. 2011.

[10] Z. Q. Zhu, N. Pothi, P. L. Xu, and Y. Ren, "Uncontrolled generator fault protection of novel hybrid-excited permanent magnet machines utilizing field excitation current control," in *Proc. 13th Int. Conf. Electr. Mach. (ICEM)*, Alexandroupoli, Greece, Sep. 2018, pp. 1724–1730.

[11] Z. Zhang, Y. Yan, S. Yang, and Z. Bo, "Principle of operation and feature investigation of a new topology of hybrid excitation synchronous machine," *IEEE Trans. Magn.*, vol. 44, no. 9, pp. 2174–2180, Sep. 2008.

[12] B. Nedjar, S. Hlioui, Y. Amara, L. Vido, M. Gabsi, and M. Lecrivain, "A new parallel double excitation synchronous machine," *IEEE Trans. Magn.*, vol. 47, no. 9, pp. 2252–2260, Sep. 2011.

[13] J. A. Tapia, F. Leonardi, and T. A. Lipo, "Consequent-pole permanent-magnet machine with extended field-weakening capability," *IEEE Trans. Ind. Electron.*, vol. 39, no. 6, pp. 1704–1709, Nov./Dec. 2003.

[14] C. Liu, K. T. Chau, J. Z. Jiang, and S. Niu, "Comparison of stator-permanent-magnet brushless machines," *IEEE Trans. Magn.*, vol. 44, no. 11, pp. 4405–4408, Nov. 2008.

[15] I. A. A. Afinowi, Z. Q. Zhu, Y. Guan, J. C. Mipo, and P. Farah, "Hybrid-excited doubly salient synchronous machine with permanent magnets between adjacent salient stator poles," *IEEE Trans. Magn.*, vol. 51, no. 10, Oct. 2015, Art. no. 8107909.

[16] H. Yang, Z. Q. Zhu, Y. Liu, H. Y. Li, and J. C. Mipo, "Comparative study of doubly salient machines with/without stator slot permanent magnets," in *Proc. IEEE Int. Electr. Mach. Drives Conf. (IEMDC)*, Miami, FL, USA, May 2017, pp. 1–6.

[17] M. J. Jin, C. F. Wang, J. X. Shen, and B. Xia, "A modular permanent-magnet flux-switching linear machine with fault-tolerant capability," *IEEE Trans. Magn.*, vol. 45, no. 8, pp. 3179–3186, Aug. 2009.

[18] S. R. Mousavi-Aghdam, M. R. Feyzi, N. Bianchi, and M. Morandin, "Design and analysis of a novel high-torque stator-segmented SRM," *IEEE Trans. Ind. Electron.*, vol. 63, no. 3, pp. 1458–1466, Mar. 2016.

[19] G. J. Li, Z. Q. Zhu, M. Foster, and D. Stone, "Comparative studies of modular and unequal tooth PM machines either with or without tooth tips," *IEEE Trans. Magn.*, vol. 50, no. 7, Jul. 2014, Art. no. 8101610.

[20] G. Heins, D. M. Ionel, and M. Thiele, "Winding factors and magnetic fields in permanent-magnet brushless machines with concentrated windings and modular stator cores," *IEEE Trans. Ind. Appl.*, vol. 51, no. 4, pp. 2924–2932, Jul. 2015.

[21] P. Andrada, B. Blanqué, E. Martínez, and M. Torrent, "New hybrid reluctance motor drive," in *Proc. 20th Int. Conf. Elect. Mach. (ICEM)*, Sep. 2012, pp. 2689–2694.

[22] W. Ding, S. Yang, Y. Hu, S. Li, T. Wang, and Z. Yin, "Design consideration and evaluation of a 12/8 high-torque modular-stator hybrid excitation switched reluctance machine for EV applications," *IEEE Trans. Ind. Appl.*, vol. 64, no. 12, pp. 9221–9232, Dec. 2017.

[23] J. A. Walker, D. G. Dorrell, and C. Cossar, "Flux-linkage calculation in permanent-magnet motors using the frozen permeabilities method," *IEEE Trans. Magn.*, vol. 41, no. 10, pp. 3946–3948, Oct. 2005.

[24] G. Zhang, M. Cheng, W. Hua, and J. Dong, "Analysis of the oversaturated effect in hybrid excited flux-switching machines," *IEEE Trans. Magn.*, vol. 47, no. 10, pp. 2827–2830, Oct. 2011.

[25] H. Akita, Y. Nakahara, N. Miyake, and T. Oikawa, "New core structure and manufacturing method for high efficiency of permanent magnet motors," in *Proc. 38th IAS Annu. Meeting Conf. Rec. Ind. Appl. Conf.*, Salt Lake, UT, USA, vol. 1, Oct. 2003, pp. 367–372.

[26] F. Libert and J. Soulard, "Manufacturing methods of stator cores with concentrated windings," in *Proc. 3rd IET Int. Conf. Power Electron., Mach. Drives (PEMD)*, Dublin, Ireland, Apr. 2006, pp. 676–680.

[27] Z. Q. Zhu, "A simple method for measuring cogging torque in permanent magnet machines," in *Proc. IEEE Power Energy Soc. Gen. Meeting*, Calgary, AB, Canada, Jul. 2009, pp. 1–4.

[28] Z. Q. Zhu, Z. Azar, and G. Ombach, "Influence of additional air gaps between stator segments on cogging torque of permanent-magnet machines having modular stators," *IEEE Trans. Magn.*, vol. 48, no. 6, pp. 2049–2055, Jun. 2012.

[29] J.-X. Shen, S. Cai, J. Yuan, S. Cao, and C.-W. Shi, "Cogging torque in SPM machine with segmented stator," *COMPEL, Int. J. Comput. Math. Elect. Electron. Eng.*, vol. 35, no. 2, pp. 641–654, 2016.